Microwave resonance in a high-quality GaAs/AlGaAs two-dimensional electron system in the low-density and low-mobility condition

R. G. Mani,[1] A. Kriisa,[1] C. Reichl,[2] and W. Wegscheider[2]
[1]*Department of Physics and Astronomy, Georgia State University, Atlanta 30303, USA*
[2]*Laboratorium für Festkörperphysik, ETH-Zürich, Zürich 8093, Switzerland*

(Received 14 May 2019; revised manuscript received 17 July 2019; published 4 October 2019)

Radiation induced magnetoresistance oscillations are well known and readily observable in the high-quality two-dimensional (2D) electron system. Here, we report unexpected photoexcited transport, under a low-carrier density, low-mobility condition, in the high-quality GaAs/AlGaAs devices that exhibit the above-mentioned oscillations. This study reveals enhanced nonresonant magnetoresistance as well as microwave resonance that appear unrelated to the above-mentioned radiation-induced magnetoresistance oscillations. The positions of the resonance along the B axis depends on the microwave power, the microwave frequency, and the direction of sweep of the magnetic field, as the photoexcited diagonal resistance is prominently enhanced over the dark value. Most remarkably, the observed microwave-induced resonance becomes unobservable below a characteristic cutoff frequency. These features suggest a bulk magnetoplasmon origin for the observed resonances. A picture including bottlenecks in transport within 2D electron systems and microwave modified tunneling at bottlenecks is suggested to help understand some aspects of experiment.

DOI: 10.1103/PhysRevB.100.155301

I. INTRODUCTION

The GaAs/AlGaAs semiconductor heterostructure system continues to be a preferred test bed for studying novel physical phenomena in two-dimensional (2D) electron systems [1] because continuing technological advances in material preparation now routinely make possible a carrier mobility well beyond the $\mu = 10^7$ cm^2/V s range. In such high-mobility material, the mean free path of carriers can approach the millimeter range due to the reduced role for impurity scattering, thereby providing for the possibility of observing size effects even in macroscopic specimens at liquid-helium temperatures [2]. A characteristic of such high-quality GaAs/AlGaAs 2D electron systems turns out to be a remarkable sensitivity of magnetotransport at liquid-helium temperatures to photoexcitation, particularly photoexcitation from the microwave, mm-wave, and terahertz bands of the electromagnetic wave spectrum [3–31], an area of interest also from the radiation-sensing perspective [13]. Here, the study of the radiation-induced zero-resistance states showed that the dark resistance observed in the absence of a magnetic field could be switched off in a small magnetic field, say $B \leqslant 1$ T, with modest intensity photoexcitation about characteristic magnetic fields $B = (4/4j + 1)B_f$, where $B_f = 2\pi f m^*/e$, $j = 1, 2, 3 \ldots$, f is the radiation frequency lying in the microwave to terahertz bands, m^* is an effective mass, and e is the electron charge, as "1/4-cycle shifted" B^{-1}-periodic oscillations in the diagonal and off-diagonal resistances follow $R \approx \exp(-\alpha/B)\sin(2\pi B_f/B)$ [3]. The B^{-1}-periodic oscillations could be understood through a number of theoretical approaches [32–46] including the (a) the scattering of electrons by phonons and impurities between Landau levels or the displacement model [32–34], (b) mechanisms based on the periodic motion of electron orbit centers under photoexcitation, or the radiation-driven electron orbit model [38,40], (c) consideration of the change of the distribution function under photoexcitation, or the in-elastic model [36], (d) a synchronization theory where magnetoresistance oscillations are generated at high harmonics $\omega/\omega_c = j > 1$ by collisions with a sharp boundary or isolated impurities, and where zero-resistance states appear at the observed values as the electron cyclotron phase becomes synchronized with the microwave phase [42,43], and (e) the recollision of cyclotron electrons from scattering centers [45].

In addition to the above-mentioned sensitivity to microwaves, mm waves, and terahertz radiation, the GaAs/AlGaAs system also exhibits a sensitivity to visible and infrared light, given that GaAs is a direct gap semiconductor with a band gap $E_G = 1.44$ eV (corresponding to a wavelength $\lambda = 844$ nm) at room temperature. Indeed, a persistent photoconductivity effect is often used to prepare the above-mentioned specimens to a high-mobility condition [47]; the preparation involves briefly exposing the specimen to photoexcitation from a red LED, which increases both the low-temperature mobility and carrier density. It turns out that, for the MBE material examined here, storing the Hall bar specimens in the dark within a warm cryostat for several days serves to reduce the carrier density well below the values observed in specimens stored under ambient conditions. Here, we report an experimental investigation of magnetotransport under microwave photoexcitation in such rarely examined dark-stored high-quality specimens. Remarkably, such specimens exhibit profound sensitivity to microwave photoexcitation and the specimen response turns out to be very different from their above-mentioned standard response in the high-mobility, high-density condition. A characteristic feature observed here in the

low-mobility, low-density condition is that the microwave photoexcited diagonal resistance is prominently enhanced over the dark value. In addition, the magnetotransport reveals microwave resonances that appear unrelated to the above-mentioned radiation-induced magnetoresistance oscillations. The positions of the resonance along the B axis depends on the direction of sweep of the magnetic field, the microwave power, and the microwave frequency. Further, this microwave induced resonance becomes unobservable below a characteristic cutoff frequency. These reported features appear consistent with a bulk magnetoplasmon effect [48–51] for the resonance phenomena. The origin of the nonresonant enhanced photomagnetoresistance and hysteretic effects remains to be clarified.

II. EXPERIMENT AND RESULTS

Devices were fabricated from GaAs/AlGaAs single heterojunctions with the 2D electron systems (2DESs) buried 320 nm below the top surface. A 70-nm spacer layer separated the 2DES from the Si doping layer, which was followed by 240 nm of AlGaAs spacer layer and a 10-nm GaAs cap layer. These GaAs/AlGaAs heterostructures were patterned into Hall bar devices [52,53] with a width $W = 200\ \mu$m by photolithography. These devices were loaded onto a waveguide sample holder with a cutoff frequency of ≈15 GHz and inserted into a liquid-helium cryostat to place the specimen at the center of a superconducting solenoid magnet. The samples were immersed in liquid helium for all the reported measurements. Magnetotransport measurements were performed using low-frequency lock-in techniques, in order to obtain the diagonal resistance R_{xx} vs the magnetic field. The linearly polarized photoexcitation was produced, over the 30–50-GHz frequency band, using commercially available synthesizers. A 6× multiplier mm-wave module served to provide radiation between 65 and 110 GHz.

Figure 1(a) shows the dark and photoexcited magnetotransport characteristics in the high-mobiity μ, high-density n condition obtained exploiting the persistent photoconductivity effect in a GaAs/AlGaAs heterostructure. Here, $n = 2.3 \times 10^{11}$ cm^{-2}/V s and $\mu = 14.5 \times 10^6$ cm^{-2}/V s. The dark traces, shown for the upsweep and downsweep conditions exhibit mostly positive magnetoresistance above $B = 0.020$ T along with Shubnikov–de Haas oscillations above $B = 0.15$ T at $T = 1.5$ K. Photoexcitation of the specimen with $f =$ 44 GHz radiation induces the radiation-induced magnetoresistance oscillations with extrema that fall above and below the dark curve. For $f = 44$ GHz, $B_f \approx 0.11$ T is marked in Fig. 1(a). Notice that B_f falls near a node, where the dark curves intersect the photoexcited traces, in the radiation-induced magnetoresistance oscillations. In sum, these results represent standard magnetotransport characteristics of the high-mobility, high-density condition, which have been well known for quite some time [3].

After the measurements shown above were carried out, the cryostat with the sample within it was allowed to warm up, in the dark, to room temperature, and maintained in that condition for several days. Subsequently, the cryostat and sample were recooled down to liquid-helium temperatures for the next set of measurements, without any photoexcitation with

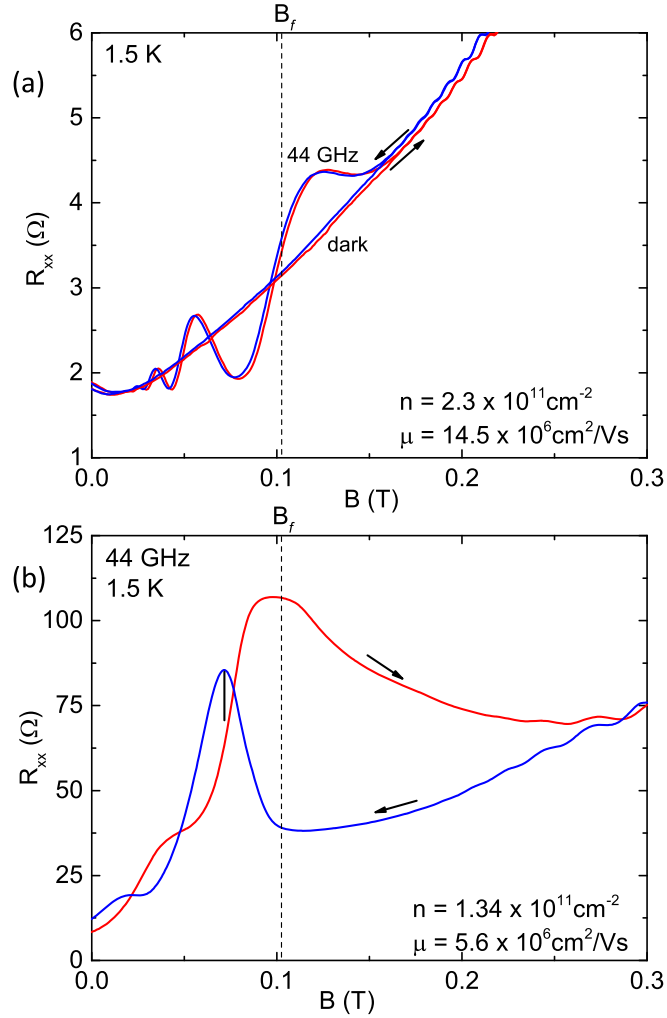

FIG. 1. (a) The dark and photoexcited diagonal resistance R_{xx} in a GaAs/AlGaAs heterostructure in the high-mobility (14.5×10^6 cm^2/V s), high-carrier density ($n = 2.3 \times 10^{11}$ cm^{-2}) condition. The red (blue) traces correspond to the upsweep (downsweep) conditions. (b) The photoexcited traces of R_{xx} in the low-mobility (5.6×10^6 cm^2/V s), low-density ($n = 1.34 \times 10^{11}$ cm^{-2}) condition. Notice the large hysteresis effect. The photoexcited traces in both (a) and (b) were obtained with $f = 44$-GHz photoexcitation. $B_f = 2\pi f m^*/e$ is the characteristic field for the radiation-induced magnetoresistance oscillations. Note that in (a) a B_f lies next to a node in the radiation-induced magnetoresistance oscillations.

visible radiation. Figure 1(b) shows measurements carried out with the specimen now exhibiting $n = 1.34 \times 10^{11}$ cm^{-2} and $\mu = 5.6 \times 10^6$ cm^2/V s with $f = 44$-GHz photoexcitation at $T = 1.5$ K. The figures shows dissimilar R_{xx} traces on the upsweep (red) and downsweep (blue) of the magnetic field. Further, a large sharp peak is observable on the downsweep as a broader peak is observable on the upsweep. The peaks in R_{xx} on the upsweep and downsweep do not occur at the same value of the magnetic field. Indeed, the observed magnetoresistance characteristics in the low-density, low-mobility condition [Fig. 1(b)] bear hardly any resemblance to the features observed in the same specimen in the high-density, high- mobility condition [Fig. 1(a)]. Yet, Shubnikov–de Haas oscillations are observed to roughly the same low-B value

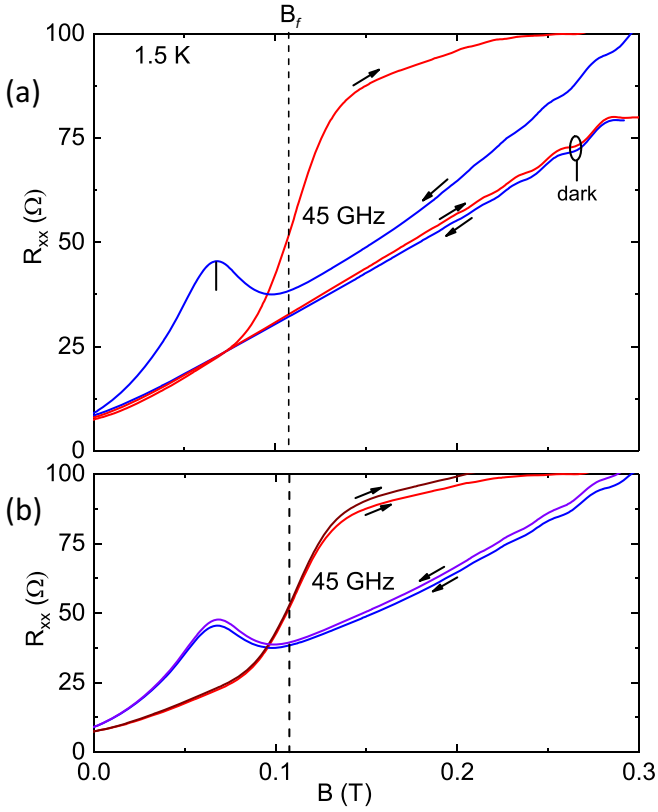

FIG. 2. (a) The dark and photoexcited magnetoresistance traces with $f = 45$-GHz photoexcitation. Note the hysteresis in the photoexcited R_{xx} traces. (b) This panel demonstrates reproducibility in the hysteresis observed in the photoexcited R_{xx} traces at $f = 45$ GHz.

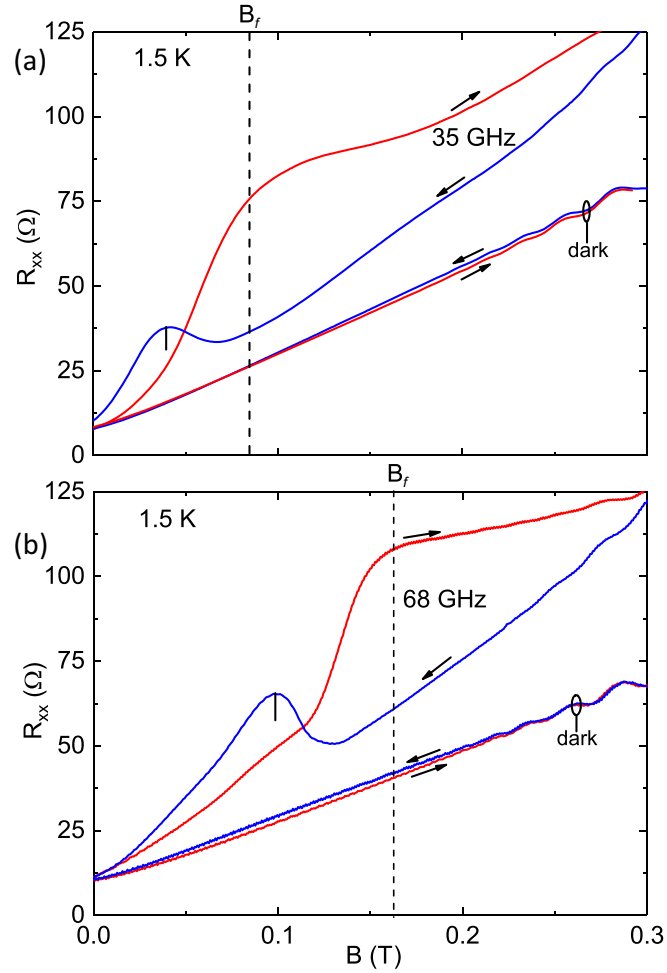

FIG. 3. (a) The dark and photoexcited magnetoresistance traces with $f = 35$-GHz photoexcitation. (b) The dark and photoexcited magnetoresistance traces with $f = 68$-GHz photoexcitation. Note that the dark traces lie well below the photoexcited traces. Further, substantial hysteresis appears in R_{xx} under photoexcitation.

(≈0.2 T) in the two cases, which testifies to the quality of the specimen even in the low-mobility condition [Fig. 1(b)].

Figure 2(a) shows dark and photoexcited magnetoresistance traces at $f = 45$ GHz. Here, the photoexcited magnetoresistance traces lie above the dark traces, especially on the downsweep of the magnetic field. Further, the observable sweep direction dependent hysteresis is pronounced in the photoexcited traces, while the dark traces look normal. Figure 2(b) shows that repeating the measurements in the photoexcited condition produces the same curves, confirming reproducibility of the observed effect.

Figure 3 compares the specimen response in the low-mobility, low-density condition at two different microwave frequencies, $f = 35$ GHz, exhibited in Fig. 3(a) and $f = 68$ GHz exhibited in Fig. 3(b), along with their associated dark traces. These panels show a sensitivity of the peak locations in B on the microwave frequency f, with the peak shifting to higher B with increasing f. In addition, these data confirm that the photoexcited magnetoresistance generally exceeds the dark magnetoresistance at different f.

Figure 4 examines the evolution of the observed resonance in the photoexcited R_{xx} as a function of the microwave power at 43.5 GHz. Figure 4(a) shows the upsweep and downsweep magnetoresistance traces with microwave source power $P = 3.16$ mW. Note once again that the resonance peak on the downsweep trace is sharper than the resonance peak on the upsweep trace. As a consequence, we exhibit the downsweep traces at a number of source power levels in Fig. 4(b), with the traces offset vertically with respect to each other for the sake of clarity. Figure 4(b) shows that the resonance peak amplitude increases with microwave power. In addition, unexpectedly, the peak position shifts to higher magnetic field with increasing P. The peak positions in B, which are marked with a vertical line segment in Fig. 4(b), are plotted as a function of P in Fig. 4(c). This figure shows that the peaks shift to higher B monotonically and nonlinearly with increasing P. A fit of the data points is given by the red line in Fig. 4(c). This fit, $B(T) = 0.0428\ \mathrm{T} + 0.019P^{0.5}(\mathrm{mW})^{0.5}$, suggests that the downsweep resonance peak shifts as the square root of the power. Since the microwave power $P \propto E^2$, these results suggest that the resonance position varies proportionately to the magnitude of the microwave electric field. This observed sensitivity to the source microwave power, shown in Figs. 4(b) and 4(c) complicates the comparison of measurements at different microwave frequencies since the coupling of microwave radiation to the specimen, via the waveguide, is not the same at all f. To make the comparison possible, we carried out power dependent measurements at various f, as

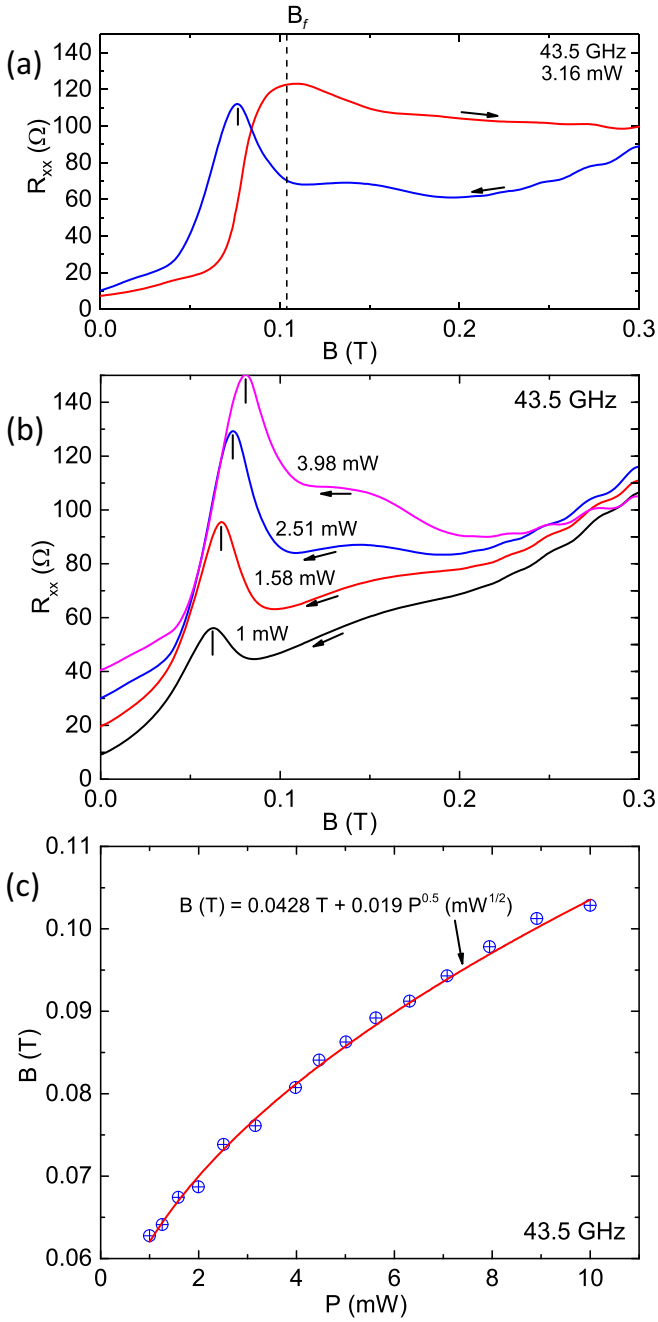

FIG. 4. (a) The photoexcited magnetoresistance R_{xx} under $f =$ 43.5-GHz photoexcitation. (b) The downsweep photoexcited magnetoresistance under $f = 43.5$-GHz photoexcitation at various radiation source-power (P) levels as shown. Notice that the largest peak in R_{xx} shifts to higher magnetic field with increased power P. (c) This panel shows the position of the largest peak in R_{xx} in (b) as a function of P. The peak shifts approximately as $P^{0.5}$, as indicated by the fit line.

in Fig. 4(b), then fit the observed resonance field position vs P as in Fig. 4(c), and extracted the $P \to 0$ value of the resonance field. In Fig. 4(c), for example, this value would be $B = 0.0428$ T.

In Fig. 5, we plot the resonance field values, as symbols, for $P \to 0$, at different f. In addition, we have fit the data points with an empirical fit, $B_R = 1.7 \times 10^{-3}[f(\mathrm{GHz})^2 - 35.1^2]^{1/2}$.

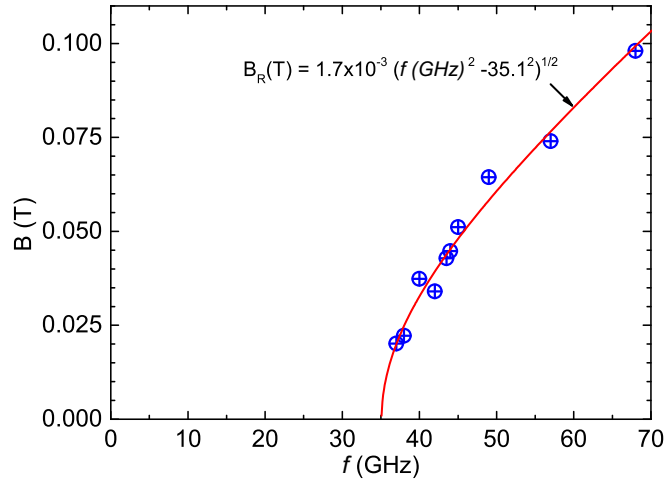

FIG. 5. The vanishing power, i.e., $P \to 0$, resonance peak positions, see Fig. 4(c), is exhibited as a function of the radiation frequency f. Note that the fit curve, shown in red, intercepts the abscissa at $B \approx 35$ GHz.

The salient features conveyed by this graph are as follows: (a) The resonance field position drops to zero at about $f =$ 35.1 GHz. This implies resonances should not be observable under photoexcitation at $f \leqslant 35.1$ GHz. Indeed, measurements confirmed the absence of such microwave induced resonance below 35 GHz. (b) The $P \to 0$ resonance field increases nonlinearly with f as $(f^2 - 35.1^2)^{1/2}$.

III. DISCUSSION AND SUMMARY

2D electrons subjected to a plane perpendicular magnetic field exhibit circular cyclotron motion perpendicular to the magnetic field in response to the Lorentz force. The angular frequency of this motion is $\omega_c = 2\pi f_c = qB/m^*$, and it is independent of the radius of the electron orbit and the electron velocity. When a circularly polarized electric field at frequency f is applied at the electron cyclotron frequency, i.e., $2\pi f = \omega_c$, with the same sense of rotation as the electron orbit, there is cyclotron resonance. The cyclotron resonance magnetic field is nominally $B_c = B_f = 2\pi f m^*/e$, defined earlier, if one identifies the effective mass entering into that B_f expression as the cyclotron effective mass. At $f = 44$ GHz, $B_c \approx 0.11$ T. For cyclotron resonance, one expects the resonances to shift to higher B linearly with the f, unlike what is observed in Fig. 4(c).

2D electron systems also support bulk plasmons—collective electron oscillations, at a frequency $f_p = (1/2\pi)(\sqrt{\frac{ne^2}{2\varepsilon_{\mathrm{eff}}\varepsilon_o m*}}k)$, where n is the electron density, e is the electron charge, $\varepsilon_{\mathrm{eff}} = 6.9$ is the effective GaAs dielectric constant [48], ε_o is the permittivity of free space, m^* is the effective mass, and k is the plasmon wave vector. For plasmon confinement within a strip of width W, the plasmon wave vector for the lowest mode $k \approx \pi/W$, where the width of sample, W, equals half the plasmon wavelength [48–51]. This bulk plasmon can hybridize with cyclotron resonance to yield the magnetoplasmon. The magnetoplasmon frequency, $f_{mp}(B) = \sqrt{(f_c)^2 + [f_p(B=0)]^2}$. By inserting

$f_c = qB/(2\pi m^*)$ into this expression, one obtains that the magnetoplasmon resonance field is $B = (2\pi m^*/e)(f_{mp}^2 - f_p^2)^{1/2}$ [48–51]. Upon comparing with the fit equation of Fig. 5, $B_R = 1.7 \times 10^{-3}[f(\mathrm{GHz})^2 - 35.1^2]^{1/2}$, it appears that the observed resonance frequencies in the $P \to 0$ limit follow expectations for the magnetoplasmon resonance in the GaAs/AlGaAs specimen. In particular, one might identify the abscissa intercept, $f = 35.1$ GHz, with the experimentally observed plasmon frequency f_p^{exp}. The observed value here may be compared with theoretical expectations $f_p^{\mathrm{th}} = (1/2\pi)(\sqrt{\frac{n_s e^2}{2\varepsilon_{\mathrm{eff}}\varepsilon_o m*}}k) = 43.4$ GHz for $n = 1.34 \times 10^{11}$ cm^{-2}, and $W = 0.2 \times 10^{-4}$ m. That is, the measured $f_p^{\mathrm{exp}} = 35.1$ GHz agrees within 20% of expected plasmon frequency, f_p^{th}. Similarly, one might compare the observed prefactor, 1.7×10^{-3} T/GHz in the fit equation $B_R = 1.7 \times 10^{-3}[f(\mathrm{GHz})^2 - 35.1^2]^{1/2}$, with expectations for the same from theory, where the prefactor should equal $(2\pi m^*/e)$ in units of T/Hz. It turns out that $(2\pi m^*/e) = 2.39 \times 10^{-12}$ T/Hz $= 2.39 \times 10^{-3}$ T/GHz, for $m^*/m = 0.067$. Thus, the measured prefactor, 1.7×10^{-3} T/GHz, agrees within 28% of the expected value, 2.39×10^{-3} T/GHz. These features suggest that the observed dispersion in Fig. 5 signifies a role for the magnetoplasmon in the observed resonances; see Figs. 1(b)–4.

There are, however, features in the experiment that require additional explanation. For example, there is a large nonresonant—in addition to the resonant—enhancement of the diagonal resistance under photoexcitation in comparison to the dark curves (see Fig. 3). Since $\mu \approx 5 \times 10^6$ cm^2/V s [see Fig. 1(b)] and, therefore, $\mu B > 1$ over the examined B range, the observed enhanced R_{xx} under photoexcitation corresponds to enhanced magnetoconductance, per standard interpretation. To understand such an enhanced magnetoconductance, we recall results from STM studies of tunneling in nanojunctions under microwave photoexcitation [54]. Such experiments showed that microwave photoexcitation of a tunnel junction can modify the tunneling current across the junction at a fixed voltage bias (as a consequence of a rectification of the applied alternating microwave electric field), signifying a modification in the tunneling conductance. Indeed, the modification in the tunneling current turned out to be a function of the microwave voltage or electric field across the junction [54]. If the GaAs/AlGaAs specimens under investigation here include lateral transport bottlenecks within the 2DES system (due to increased disorder at the examined lower carrier density) [55], one might extend that picture to this case here by suggesting that the tunneling conductance at such bottlenecks is increased by the microwave photoexcitation, leading to enhanced nonresonant magnetoconductance and magnetoresistance under photoexcitation. It could be that under magnetoplasmon resonance, the tunneling conductance at these bottlenecks is resonantly further enhanced, leading to a large magnetoplasmon resistance peak, as the plasmon ramifies across the specimen. Note that the magnetoresistance data exhibit large hysteresis effects; see Fig. 1(b). There is also the power dependence in the positions of the resonances; see Fig. 4(b). Experiment also suggests the existence of a time constant in the problem; see Fig. 6. In Fig. 6, it can be seen that the magnitude of the hysteresis between the upsweep and downsweep traces depends on the sweep rate. Also, the peak positions depend on the sweep rate. The postpeak drop in the resistance on the upsweep traces clearly suggest an *RC*-type time constant in the problem. Perhaps such a time constant should be associated with a charging effect. All the observed features taken together point to the possible existence of such transport bottlenecks, which are perhaps defined by charged defects, with tunneling at these bottlenecks sensitively depending upon the microwave electric field. Perhaps increasing the photoexcitation somehow even increases the effective density locally in the area of the defects, leading to a shift in the observed magnetoplasma frequency with the microwave power, and the observations shown in Fig. 4(b). There are theoretical studies which suggest that intense microwave excitation leads to the trapping of carriers in the vicinity of defects [43,45]. Perhaps such ideas merit consideration in the explanation of these experimental observations.

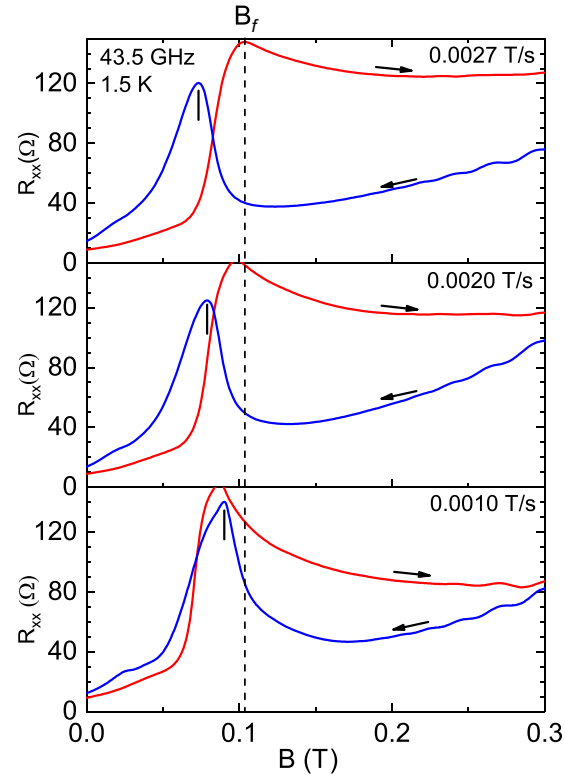

FIG. 6. This figure shows the diagonal magnetoresistance R_{xx} vs B at B-sweep rates. Top: 0.0027 T/s; center: 0.0020 T/s; bottom: 0.0010 T/s. Note that the shift in the locations of the major peak on the upsweep and downsweep traces is sensitive to the sweep rate. In addition, the magnitude of the hysteresis between the upsweep and downsweep traces depends also on the sweep rate. In these experiments, the hold time at $B = 0.3$ T was the same for all three measurements.

In summary, photoexcited transport in the high-quality, low-density, low-mobility GaAs/AlGaAs specimen under microwave photoexcitation reveals a nonresonant diagonal resistance enhancement in addition to what appears to be a different sort of microwave induced resonance, one which distinctly differs from the microwave radiation induced magnetoresistance oscillations [3,4] observed in the same

specimens under the high-density, high-mobility conditions. Various features in the resonant aspects of the phenomena, such as the observed dispersion, see Fig. 5, strongly correlate with a magnetoplasmon origin [48–51]. At the same time, other features suggest a role for charging, perhaps at defects, which remains to be better understood.

ACKNOWLEDGMENTS

The magnetotransport work was supported by the NSF under ECCS 1710302. Microwave, mm-wave, and terahertz work was supported by the Army Research Office under W911NF-15-1-0433.

[1] T. Ando, A. B. Fowler, and F. Stern, Rev. Mod. Phys. **54**, 437 (1982).

[2] R. G. Mani, A. Kriisa, and W. Wegscheider, Sci. Rep. **3**, 2747 (2013).

[3] R. G. Mani, J. H. Smet, K. von Klitzing, V. Narayanamurti, W. B. Johnson, and V. Umansky, Nature (London) **420**, 646 (2002); Phys. Rev. Lett. **92**, 146801 (2004); Phys. Rev. B **69**, 193304 (2004).

[4] M. A. Zudov, R. R. Du, L. N. Pfeiffer, and K. W. West, Phys. Rev. Lett. **90**, 046807 (2003).

[5] R. G. Mani, V. Narayanamurti, K. von Klitzing, J. H. Smet, W. B. Johnson, and V. Umansky, Phys. Rev. B **69**, 161306(R) (2004); **70**, 155310 (2004).

[6] A. E. Kovalev, S. A. Zvyagin, C. R. Bowers, J. L. Reno, and J. A. Simmons, Solid State Commun. **130**, 379 (2004).

[7] I. V. Kukushkin, M. Y. Akimov, J. H. Smet, S. A. Mikhailov, K. von Klitzing, I. L. Aleiner, and V. I. Falko, Phys. Rev. Lett. **92**, 236803 (2004).

[8] R. G. Mani, Physica E (Amsterdam, Neth.) **22**, 1 (2004); **40**, 1178 (2008); Appl. Phys. Lett. **85**, 4962 (2004); Phys. Rev. B **72**, 075327 (2005); Appl. Phys. Lett. **91**, 132103 (2007); Int. J. Mod. Phys. B **18**, 3473 (2004); Solid State Commun. **144**, 409 (2007).

[9] B. Simovič, C. Ellenberger, K. Ensslin, H.-P. Tranitz, and W. Wegscheider, Phys. Rev. B **71**, 233303 (2005).

[10] J. H. Smet, B. Gorshunov, C. Jiang, L. Pfeiffer, K. West, V. Umansky, M. Dressel, R. Meisels, F. Kuchar, and K. von Klitzing, Phys. Rev. Lett. **95**, 116804 (2005).

[11] S. A. Studenikin, A. S. Sachrajda, J. A. Gupta, Z. R. Wasilewski, O. M. Fedorych, M. Byszewski, D. K. Maude, M. Potemski, M. Hilke, K. W. West, and L. N. Pfeiffer, Phys. Rev. B **76**, 165321 (2007).

[12] S. Wiedmann, G. M. Gusev, O. E. Raichev, T. E. Lamas, A. K. Bakarov, and J. C. Portal, Phys. Rev. B **78**, 121301(R) (2008).

[13] R. G. Mani, Appl. Phys. Lett. **92**, 102107 (2008).

[14] R. G. Mani, W. B. Johnson, V. Umansky, V. Narayanamurti, and K. Ploog, Phys. Rev. B **79**, 205320 (2009).

[15] S. Wiedmann, N. C. Mamani, G. M. Gusev, O. E. Raichev, A. K. Bakarov, and J. C. Portal, Phys. Rev. B **80**, 245306 (2009).

[16] R. G. Mani, C. Gerl, S. Schmult, W. Wegscheider, and V. Umansky, Phys. Rev. B **81**, 125320 (2010).

[17] S. Wiedmann, G. M. Gusev, O. E. Raichev, A. K. Bakarov, and J. C. Portal, Phys. Rev. B **82**, 165333 (2010).

[18] D. Konstantinov and K. Kono, Phys. Rev. Lett. **105**, 226801 (2010).

[19] R. G. Mani, A. N. Ramanayaka, and W. Wegscheider, Phys. Rev. B **84**, 085308 (2011).

[20] A. N. Ramanayaka, R. G. Mani, and W. Wegscheider, Phys. Rev. B **83**, 165303 (2011).

[21] A. N. Ramanayaka, R. G. Mani, J. Inarrea, and W. Wegscheider, Phys. Rev. B **85**, 205315 (2012).

[22] R. G. Mani, A. N. Ramanayaka, T. Ye, M. S. Heimbeck, H. O. Everitt, and W. Wegscheider, Phys. Rev. B **87**, 245308 (2013).

[23] R. G. Mani and A. Kriisa, Sci. Rep. **3**, 3478 (2013).

[24] T. Ye, H. C. Liu, W. Wegscheider, and R. G. Mani, Phys. Rev. B **89**, 155307 (2014).

[25] A. D. Chepelianskii, N. Watanabe, K. Nasyedkin, K. Kono, and D. Konstantinov, Nat. Commun. **6**, 7210 (2015).

[26] T. Ye, H.-C. Liu, Z. Wang, W. Wegscheider, and R. G. Mani, Sci. Rep. **5**, 14880 (2015).

[27] H.-C. Liu, R. L. Samaraweera, R. G. Mani, C. Reichl, and W. Wegscheider, Phys. Rev. B **94**, 245312 (2016).

[28] Z. Wang, R. L. Samaraweera, C. Reichl, W. Wegscheider, and R. G. Mani, Sci. Rep. **6**, 38516 (2016); R. L. Samaraweera, H.-C. Liu, B. Gunawardana, A. Kriisa, C. Reichl, W. Wegscheider, and R. G. Mani, *ibid.* **8**, 10061 (2018).

[29] R. L. Samaraweera, H.-C. Liu, Z. Wang, C. Reichl, W. Wegscheider, and R. G. Mani, Sci. Rep. **7**, 5074 (2017).

[30] T. R. Nanayakkara, R. L. Samaraweera, B. Gunawardana, C. R. Munasinghe, A. Kriisa, R. G. Mani, C. Reichl, and W. Wegscheider, Phys. Rev. B **98**, 035304 (2018).

[31] H.-C. Liu, C. Reichl, W. Wegscheider, and R. G. Mani, Sci. Rep. **8**, 7878 (2018).

[32] A. C. Durst, S. Sachdev, N. Read, and S. M. Girvin, Phys. Rev. Lett. **91**, 086803 (2003).

[33] V. Ryzhii and R. Suris, J. Phys.: Condens. Matter **15**, 6855 (2003).

[34] X. L. Lei and S. Y. Liu, Phys. Rev. Lett. **91**, 226805 (2003); Phys. Rev. B **72**, 075345 (2005); **86**, 205303 (2012).

[35] S. A. Mikhailov, Phys. Rev. B. **70**, 165311 (2004).

[36] I. A. Dmitriev, M. G. Vavilov, I. L. Aleiner, A. D. Mirlin, and D. G. Polyakov, Phys. Rev. B **71**, 115316 (2005).

[37] M. Torres and A. Kunold, Phys. Rev. B **71**, 115313 (2005).

[38] J. Inarrea and G. Platero, Phys. Rev. Lett. **94**, 016806 (2005); Phys. Rev. B **72**, 193414 (2005).

[39] O. E. Raichev, Phys. Rev. B **78**, 125304 (2008).

[40] J. Iñarrea, Appl. Phys. Lett. **92**, 192113 (2008); **100**, 242103 (2012); J. Appl. Phys. **113**, 183717 (2013).

[41] J. Inarrea, R. G. Mani, and W. Wegscheider, Phys. Rev. B **82**, 205321 (2010).

[42] A. D. Chepelianskii and D. L. Shepelyansky, Phys. Rev. B **80**, 241308(R) (2009).

[43] O. V. Zhirov, A. D. Chepelianskii, and D. L. Shepelyansky, Phys. Rev. B **88**, 035410 (2013).

[44] O. E. Raichev, Phys. Rev. B **91**, 235307 (2015).

[45] Y. M. Beltukov and M. I. Dyakonov, Phys. Rev. Lett. **116**, 176801 (2016).

[46] C.-C. Chang, G.-Y. Chen, and L. Lin, Sci. Rep. **6**, 37763 (2016).

[47] R. G. Mani and J. R. Anderson, Phys. Rev. B **37**, 4299 (1988).

[48] E. Vasiliadou, G. Muller, D. Heitmann, D. Weiss, K. von Klitzing, H. Nickel, W. Schlap, and R. Losch, Phys. Rev. B **48**, 17145 (1993).

[49] I. V. Kukushkin, V. M. Muravev, J. H. Smet, M. Hauser, W. Dietsche, and K. von Klitzing, Phys. Rev. B **73**, 113310 (2006).

[50] V. M. Muravev, C. Jiang, I. V. Kukushkin, J. H. Smet, V. Umansky, and K. von Klitzing, Phys. Rev. B **75**, 193307 (2007).

[51] A. Kriisa, R. L. Samaraweera, M. S. Heimbeck, H. O. Everitt, C. Reichl, W. Wegscheider, and R. G. Mani, Sci. Rep. **9**, 2409 (2019).

[52] R. G. Mani and K. von Klitzing, Appl. Phys. Lett. **64**, 1262 (1994); **64**, 3121 (1994); Z. Phys. B **92**, 335 (1993); Phys. Rev. B **46**, 9877 (1992); Z. Phys. B **100**, 635 (1996).

[53] R. G. Mani, J. Phys. Soc. Jpn. **65**, 1751 (1996); Phys. Rev. B **55**, 15838 (1997); Appl. Phys. Lett. **70**, 2879 (1997); Physica E (Amsterdam, Neth.) **12**, 152 (2002).

[54] X. W. Tu, J. H. Lee, and W. Ho, J. Chem. Phys. **124**, 021105 (2006).

[55] M. A. Topinka, B. J. Leroy, R. M. Westervelt, S. E. J. Shaw, R. Fleischmann, E. J. Heller, K. D. Maranowski, and A. C. Gossard, Nature (London) **410**, 183 (2001).